BBA - Biomembranes 1868 (2026) 184525

Contents lists available at ScienceDirect

BBA - Biomembranes

journal homepage: www.elsevier.com/locate/bbamem

Mechanisms of blood-brain barrier penetration: A molecular dynamics study on R9 and MPG peptide translocation☆

Cintia Emi Yanaguibashi Leal [a], Nicola D'Amelio [a], Benjamin Bouvier [a,*]

[a] Unité de Génie Enzymatique et Cellulaire, UMR CNRS 7025, UFR des Sciences, Université de Picardie Jules Verne, 33 rue Saint Leu, 80039, Amiens Cedex 1, France

ARTICLE INFO

Keywords:
Cell-penetrating peptides
Blood-brain-barrier
Molecular dynamics
Membrane translocation

ABSTRACT

One of the major obstacles in treating diseases that affect the central nervous system is delivering drugs across the blood-brain-barrier (BBB). Cell-penetrating peptides (CPPs) can be used as delivery vectors, but their translocation mechanism is still poorly understood, in part due to the simplistic membrane models applied to their interpretation. Here we investigate the translocation mechanism of two CPPs, R9 and MPG, using molecular dynamics and enhanced sampling techniques on a realistic membrane model of human brain microvascular endothelial cells. The results suggest that R9 induces greater membrane disruption compared to MPG, yet that both face a significant free energy barrier to translocation. In both peptides the first interactions were initiated by the N-terminus and prominently involved arginine residues even for MPG. The crucial role of the plasticity of both partners (BBB bending, partial CPP unfolding) on the translocation energetics was also explored by sampling ad hoc collective variables, revealing the important role of long polyunsaturated acyl chain lipids. Together, these findings provide mechanistic insight into CPP-mediated transport and offer guidelines for rational design.

1. Introduction

Recent epidemiological data estimate that approximately 43% of the global population is affected by a nervous system disorder. Among these individuals, about 85% suffer from diseases that directly affect the central nervous system [1]. This highlights the urgent need for effective therapeutic interventions. For decades, the efficient delivery of drugs to the brain has been a significant obstacle in neuroscience and pharmacology, primarily due to the protective nature of the blood-brain barrier (BBB) [2,3].

The BBB is a specialized structure that regulates the passage of substances between the bloodstream and the central nervous system to maintain an optimal neuronal environment. It is primarily composed of endothelial cells (ECs), a basal lamina, pericytes, and astrocytes [4]. The ECs form a hydrophobic layer with low transcytosis rates, and are connected to one another by tight junctions, which prevent paracellular transport [5]. Pericytes are mural cells that regulate capillary function and exhibit phagocytic activity [6]. Astrocytic endfeet promote EC specialization and can upregulate genes involved in efflux mechanisms [7,8]. These three cell types adhere to the basal lamina, a three-dimensional network of glycoproteins and proteoglycans that stabilizes the cellular architecture and provides an additional physical barrier limiting molecular entry into the brain [9]. Together, these complementary functions restrict passive diffusion across the BBB to only small (<400 Da), highly lipophilic molecules, effectively excluding approximately 98% of small-molecule drugs [10]. Given this organization, ECs represent the first major physical barrier that must be crossed and are therefore the focus of this study. Their composition has been determined [11]: while the BBB shares the fundamental zwitterionic (PC/SM) outer and anionic/conical (PS/PE) inner asymmetry of typical eukaryotic plasma membranes, the BBB is uniquely enriched in lipids with polyunsaturated acyl chains. While this lipid environment biologically serves to suppress vesicular transcytosis, biophysically, the high degree of unsaturation has repercussions on the conformational flexibility of the lipid headgroups and their recognition by interfering molecules [12].

Cell-penetrating peptides (CPPs) are valuable tools that can address the difficulties imposed by the ECs [10]. CPPs are a diverse group of short sequences of amino acids (typically between 5 and 30 residues) capable of efficiently traversing biological membranes while maintaining membrane integrity. Due to the wide variety of existing CPPs, there

☆ This article is part of a Special issue entitled: 'Cellular Membranes' published in BBA - Biomembranes.

* Corresponding author.
E-mail address: benjamin.bouvier@u-picardie.fr (B. Bouvier).

https://doi.org/10.1016/j.bbamem.2026.184525
Received 16 December 2025; Received in revised form 17 March 2026; Accepted 21 March 2026
Available online 22 March 2026

is no rule for classifying them. However, the most widely adopted categorization is from a physicochemical perspective, where CPPs can be divided into cationic, amphipathic, and hydrophobic [13]. Although their effectiveness as vectors for the delivery of molecules across the BBB [14–16], the precise translocation mechanisms of CPPs remain incompletely understood and occasionally controversial [17]. One reason for this is the lack of molecular insights into peptide-lipid interactions and the thermodynamics of the translocation process, details that often cannot be grasped experimentally [18]. In such cases, molecular dynamics (MD) and related techniques have proved to be valuable alternatives for filling this gap [19–21].

However, one of the main drawbacks of using these techniques in this context is the very low likelihood of observing spontaneous translocation of a CPP in a conventional MD simulation, which progresses through femtosecond timesteps [22] while the CPP translocation experimentally occurs in minutes or more [23]. These slow kinetics are due to a complex underlying free energy profile, with minima separated by high energy barriers making it difficult to properly sample the entire translocation process under Boltzmann sampling conditions [24]. To overcome this problem, enhanced sampling techniques are extensively used [25–27].

The most popular enhanced sampling techniques rely on the identification of appropriate collective variables (CVs), which are parameters that can differentiate between the important metastable states along the putative pathway of the process under study [28]. The CVs that best describe a complex biochemical process are usually not known from the outset, and defining them is not a trivial task [29]. Hence, it is common to use more than one CV, covering different collective degrees of freedom that are empirically known to be important.

Coarse-grained (CG) representations are another way of accelerating conformational sampling. Typical CG models for biomolecules reduce the system complexity by replacing a group of 3 or 4 atoms by a single interaction site or “bead”, whose parameters are chosen to preserve the essential physicochemical properties of the original atomic group [30]. This simplification has implications for the accuracy of the results; however, it also considerably extends accessible sampling times, which are essential for the quantitative characterization of complex large-scale motions, by simultaneously simplifying the underlying free energy surfaces and reducing computational costs. The combination of enhanced sampling and coarse graining can accelerate sampling by 3 to 4 orders of magnitude (assuming a suitable choice of CV), which is especially valuable for large systems with slow conformational transitions. Its application to investigate peptide translocation mechanism is still novel despite a few recent proofs of concept [31–34].

The objective of this study is to investigate the mechanisms of CPP translocation through a realistic, experimentally-validated CG model of the BBB [35] which has never been used in this context, focusing on how each peptide's intrinsic properties influence binding, insertion, and local membrane remodeling. Although CPPs in vivo often act collectively, studying single peptides is essential to isolate their intrinsic peptide–membrane interactions. When simulating multiple CPPs together, many variables are introduced simultaneously, making it difficult to distinguish effects arising from peptide–membrane interactions from those due to peptide–peptide interactions. Building on this mechanistic framework, we go beyond previous studies, as most simulations rely on simplified membrane models [36–38] that cannot capture the compositional complexity of the BBB, including heterogeneous lipids, elevated cholesterol content, and polyunsaturated species.

To achieve this goal, we employ the MARTINI coarse-grained force field (widely used and validated for lipids, peptides, and proteins) [30,39] which we combine with enhanced sampling simulations along conformational coordinates related to membrane translocation, membrane bending, and CPP unfolding. We select two CPPs: a nona-arginine sequence (R9) and MPG, a chimeric peptide combining an HIV-1 fusion domain with an SV40 nuclear localization sequence (GALFLGFLGAAGSTMGAWSQPKKKRKV). These CPPs are both widely studied but have distinct properties: cationic, short, flexible, prone to endocytosis and cargo-agnostic for R9 [40] vs primary amphipathic, long, structured, not susceptible to endocytosis and rather cargo-specific for MPG [41]. To the best of our knowledge, this is the first CPP translocation study employing a BBB membrane model with such compositional realism. By providing a detailed characterization of CPP–BBB interaction dynamics over extended timescales, this study offers a mechanistic framework that may facilitate the rational design of optimized BBB-penetrating peptides for CNS drug delivery.

2. Computational methods

2.1. Simulations parameters and tools

Peptide structures were initially retrieved from the ADAPTABLE database [42]. After a 400 ns all-atom simulation in water using the CHARMM36 force field [43], the peptides were converted to their CG representations following the standard CHARMM-GUI protocol [43–45] (Fig. S1). The MARTINI2 CG force field [30,39] was used instead of the newer MARTINI3 model [46] following reports that the latter does not perform better than the former on the simulation of transmembrane peptides [47], and because of the much larger number of lipids that have been parameterized and validated in the older version (especially unusual lipids such as those found in the BBB). The membrane starting structure was constructed similarly. This study uses a 9-component, symmetrical membrane model by Wang et al. [35] that closely replicates the physiological lipid composition of a human brain microvascular endothelial cell: the average length of the hydrocarbon chain (18.4 carbon atoms) and number of double bonds (1.5) of the fatty acid tails both match their experimental counterparts. The total number of lipids was 510, distributed as N-oleoyl-d-erythro-sphingosylphosphorylcholine (OSM) (96), cholesterol (CHOL) (150), 1-palmitoyl-2-oleoyl-sn-glycero-3-phosphocholine (POPC) (22), 1-stearoyl-2-arachidonoyl-sn-glycero-3-phosphocholine (SAPC) (42), 1-stearoyl-2-arachidonoyl-sn-glycero-3-phosphoethanolamine (SAPE) (74), 1-stearoyl-2-oleoyl-sn-glycero-3-phosphoethanolamine (SOPE) (32), 1-stearoyl-2-arachidonoyl-sn-glycero-3-phospho-L-serine (SAPS) (42), 1-stearoyl-2-linoleoyl-sn-glycero-3-phosphocholine (SLPC) (42), and 1-stearoyl-2-arachidonoyl-sn-glycero-3-phosphoinositol (SAPI) (10) (See Table S1 for structural details). Despite slightly diverging compositions, the apical and basolateral bilayers were found by Wang et al. to have identical trans-bilayer density profiles and similar permeation rate constants for all tested compounds, in agreement with their experimental determination on an in vitro BBB model. Thus, only the apical bilayer was considered in our simulations. All systems were submitted to energy minimization until convergence.

MD simulations used a velocity-rescaling thermostat to maintain the system at 300 K, using a time constant of 1.0 ps and coupling CPP, membrane and solvent to separate heat baths. The system pressure was kept constant at 1 bar using semi-isotropic Parrinello-Rahman scheme (time constant 12.0 ps, compressibility 3.10^{-4} bar^{-1}). Long-range interactions were treated with a reaction-field approach for electrostatics (relative dielectric constant of 15) and potential-shift Verlet scheme for Van der Waals, both using a 1.1 nm cutoff. A time step of 10 fs was used for the integration, and the systems were simulated either in water (neutralized with Na^+ and Cl^- counterions) or in octane. The corresponding salt concentration was 180 mM and very close to both the experimental concentration and that used by Wang et al. [35]. The final box dimensions were approximately $12 \times 12 \times 9$ nm^3.

MD simulations were performed using Gromacs [109] versions 2023.2 and 2024.2, compiled with PLUMED 2.9.2 [50] for enhanced sampling.

2.2. CPP translocation simulations

To estimate the free energy barrier for a single CPP to translocate

through the bilayer, we selected as CV the distance along the z-axis (orthogonal to the membrane plane) between the center of mass (COM) of the peptide and the local COM of the membrane. The latter was computed as the COM of all lipid beads inside a cylinder of radius 2 nm, aligned along the z axis and centered at the peptide COM [31].

Umbrella sampling (US) simulations were performed along this CV to sample the CPP translocation mechanisms and obtain the associated free energy profiles. US is an enhanced sampling technique that applies biasing potentials centered at different values of a CV spanning the entire reaction path [51]. Independent simulations (called windows) are carried out restraining the system around each CV value, and the resulting data are then combined by methods like the weighted histogram analysis method (WHAM) to reconstruct the free energy profile along the reaction coordinate [52]. Statistical uncertainties were estimated via bootstrap resampling within WHAM, and error bars represent the standard deviation over 200 bootstrap trials [52]. To obtain reasonable starting structures for the US windows, we first pulled the peptide across the membrane along the previously defined CV, with values ranging approximately from 3.0 to −3.0 nm, at a rate of ~0.02 nm ns^{-1} and using a 1000 kJ mol^{-1} nm^{-2} restoring force. Pulling simulations can be compared to atomic force microscopy (AFM), an experimental technique in which a cantilever tip physically pulls a molecule. The main distinction lies in the pulling rate: because of computational constraints, MD simulations are up to eight orders of magnitude faster than AFM experiments, which results in higher membrane disruption in silico [53]. Nonetheless, sufficiently long US windows should allow the relaxation of such rate-dependent artifacts.

Forty structures, uniformly spaced in terms of CV and spanning the entire translocation process, were extracted from the pulling simulation and used as starting conformations for the US windows. Each of these was employed to initiate an independent 100 ns US simulation, in which the peptide was restrained along the CV using a 1000 kJ mol^{-1} nm^{-2} harmonic force. Convergence of the free energy surface was assessed by dividing the trajectory into equal time blocks and verifying the stability of the resulting profiles over them (Fig. S2). For a more detailed analysis of the CPP-membrane interactions, 150 uniformly distributed frames from the last quarter of relevant US windows were converted to the CHARMM36 all-atom representations using the “backward” backmapping tool [54].

Dedicated GROMACS tools were used for hydrogen bond and water and cholesterol density analyses at the critical points of the translocation process. Hydrogen bonds are represented as the ratio between the total number of bonds identified and the total number of frames, expressed as a percentage. Values greater than 100% reflect the occurrence of multiple simultaneous bonds between the same pairs of residues in individual frames of the trajectory. The LiPyphilic toolkit [55] was used to further investigate the translocation-induced leaflet changes of membrane lipids.

2.3. CPP folding/unfolding simulations

The radius of gyration (Rg) of the CPP backbone beads (a measure of the distribution of beads around the center of mass) was used to quantify the relative folding state of the CPPs. Because of the MARTINI model's incapacity to explicitly represent hydrogen bonds, the secondary structure of CPPs, defined based on the all-atom representation, needs to be frozen using high-modulus harmonic constraints which preclude any folding or unfolding event [30]. To address this issue, the GoMartini model was applied to CPPs beads. In this extension to MARTINI, the harmonic potentials that impose secondary structure in conventional simulations are replaced with Lennard-Jones interactions, allowing for the dynamic formation and rupture of interactions, thereby enabling the sampling of folding-unfolding transitions [56]. While GoMartini cannot compete with an all-atom model's representation of the relative statistical weights of folded and unfolded conformations, it is a valuable step forward in our search of the best accuracy-to-sampling times tradeoff.

To accelerate the slow folding/unfolding process to simulation-compatible timescales and evaluate the associated free energy barriers, well-tempered metadynamics (WTM) [57] was employed. In this approach, a history-dependent, adaptive bias is applied in the CV space, gradually filling free-energy basins with repulsive potential. The bias deposition decreases over time, ensuring smooth convergence while allowing controlled exploration of different CV values.

To compare folding behavior of CPPs under different environmental conditions, WTM simulations were conducted in aqueous solution (1 μs), octane (1 μs), and in the presence of a membrane (2 μs). For the latter, two key positions of the CPP relative to the membrane were explored: close to the membrane and adsorbed onto it. Hydrogen bonds were computed as previously, and secondary structure was evaluated with the DSSP algorithm [58]. The parameters for the WTM simulations were chosen after systematic testing (Table S2 for details), and free energy profile convergence was verified as described in Section 2.2 (Fig.S3-S4).

2.4. Membrane bending simulations

CPPs are known for promoting curvature in membranes [59,60]. To explore the influence of the CPPs on the membrane bending thermodynamics, we applied WTM simulations to a CV previously developed in our lab [61], which represents the overall curvature of a membrane patch using a single variable Γ. Γ measures the mean-square deviation of the local Gaussian curvatures at all atoms on the membrane surface, compared to a reference conformation of the same membrane (usually taken to be the “flat”, equilibrated state of the isolated membrane in which curvature is minimal). The accurate computation of local atomic curvatures is ensured by adaptively resizing the atomic neighborhoods on which they are computed, and meaningful mean-square deviations are obtained by taking into account the migration of individual lipids relative to one another between the current and the reference conformations. Enhanced sampling simulations of BBB bending were conducted in the absence and presence of a CPP. The comparison of membrane bending energetics in both cases should allow for the isolation of the peptide's influence. The parameters for WTM simulations and free energy convergence checks are available in Table S3 and Fig. S5.

3. Results and discussion

Previous translocation studies have highlighted the importance of analyzing multiple states along the CV to obtain a more comprehensive understanding of the translocation mechanism, particularly those near the highest free energy barrier [18,25]. For this purpose, three representative intermediate positions were selected, corresponding to the CPP being (A) adsorbed on the membrane surface, (B) inserted into the hydrophobic core, and (C) at the head of the opposite leaflet. For brevity, states A, B and C will be named as such throughout this section.

3.1. Translocation free energies of MPG and R9 through the BBB

We employed the US technique to estimate the free energy profile associated with the translocation process across the BBB and identify key interactions with membrane lipids. Notably, the free energy profiles for both CPPs exhibit pronounced increases as the CPP penetrates the hydrophobic core, with barrier heights reaching 250 kcal mol^{-1} despite state-of-the-art, microsecond-timescale sampling of the US windows (Fig. 1). Comparison with existing results is delicate: on the experimental front, the crossing of membranes by CPP can utilize a variety of mechanisms depending on the nature of the membrane, that of the peptide and its concentration, with limited visibility for the experimentalist on the mechanism actually taking place [62]. On the computational front, the granularity of the model (all-atom or coarse-grained), the enhanced sampling method and the collective coordinate to which it is applied all condition the barrier height. In particular, the collective coordinate defines the conformational volume accessible to the system

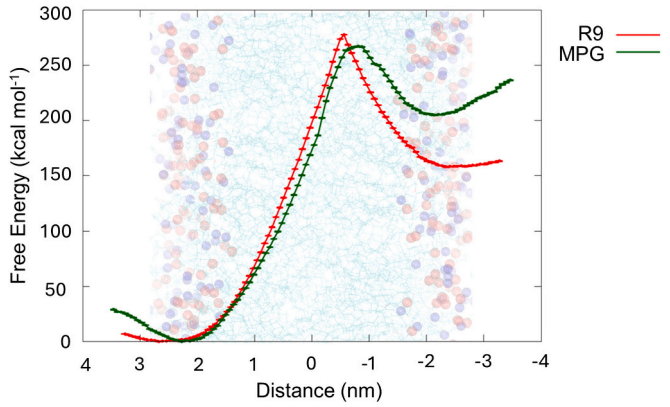

Fig. 1. Free energy of translocation of R9 (red) and MPG (green) across the BBB. Error bars represent the standard deviation estimated from 200 bootstrap trials.

during the translocation process, and no guarantee can be obtained that it encompasses the regions of lowest free energy, let alone the actual (unknown) pathway.

Most theoretical studies investigating the mechanism of CPPs are carried out with single-component model lipid bilayers [36–38]. Using a simple projection of the distance between CPP and membrane centers of mass, Kumara et al. [33] obtained a barrier of 31 kcal mol^{-1} with a coarse-grained model of R10 and a DOPC bilayer; Kabelka et al. [31] found 40 kcal mol^{-1} using a collective variable very similar to our own and a coarse-grained model of Buforin II and POPC bilayer. While such barrier heights appear lower than ours, they are extremely high in absolute, with crossing timescales of 10^8 years under the Eyring-Polanyi theory [63].

Moving on to more realistic multicomponent models is essential to correctly reproduce the properties of biological membranes, which also condition their interactions with CPPs [64]. Catalina-Hernandez et al. [26] simulated several CPPs in different membrane models consisting of DPPC, DPPC:DOPC:CHOL and DPPC:DOPC:DPPS:DOPS:CHOL using an all-atom model. They reported average translocation barrier heights of 226 kcal mol^{-1} for the multicomponent membranes and concluded that bilayer complexity is positively correlated with the free energy penalty to crossing. This correlation was also observed by Gimenez-Dejoz and Numata [21] for the translocation of five CPPs (including R9) across DPPC and DPPC:DOPC:CHOL membranes, with barriers of up to 160 kcal mol^{-1} for the latter; they also confirmed the preestablished assessment that cholesterol tends to stiffen the membrane and impair the translocation of CPPs [65–67]. Considering the complexity of our BBB model and its high cholesterol content, the barrier heights we obtained are in line with existing studies; in fact, the reduced permeability of the BBB compared to other simpler model membranes is well documented for drug-like molecules [68].

As previously mentioned, the timescales associated with such large barriers have no chance to be overcome at usual temperatures. From the computational point of view, the MARTINI2 particles are known to be too attractive, resulting in an overestimation of interaction energies which is well documented for membrane-protein interactions [69] and could contribute to artefactually high free energy barriers to CPP translocation. However, this effect is at least partially compensated by the overall acceleration of conformational motion due to the removal of high-frequency modes in MARTINI compared to all-atom, which limits the "ruggedness" of the underlying free energy landscape – this is attested by the similarly high barriers found in the previously cited all-atom simulations. Clearly, considering the variety of CPPs, membranes and computational methods covered in the available literature, the barrier heights cannot be solely attributed to modeling errors. On the contrary, they most likely indicate that the unassisted, spontaneous translocation of a single peptide is not the preferred internalization mechanism for CPPs. While this mechanism in bilayers is currently believed to be non-enzymatic [70,71] it probably involves the formation of durable pores [12,72,73], inverted micelles [72,74] and transient prepores [75] via the collective action of multiple CPPs via the collective action of multiple CPPs. Additional mechanisms may include the "masking" of peptide charges through the formation of complexes with amphiphilic molecules [76] or the modulation of membrane potential [77,78]. In the cellular context, energy-dependent assisted transport (macropinocytosis, clathrin-mediated…) can take place [62] – all of which can circumvent the barriers and are thus more likely to occur. However, these complex, multipartner mechanisms, which often overlap each other, are mostly beyond the scope of free energy methods even using coarse-grained representations; because of this, in-depth studies of individual CPP-membrane interactions such as ours and those cited above retain value as the fundamental ingredients involved in these more complex real-life internalization processes.

Finally, a difference of approximately 10 kcal mol^{-1} between the barriers can be observed. Interestingly, Catalina-Hernandez et al. [26] report qualitatively similar behavior, with barriers of 226.9 kcal mol^{-1} for R9 and 254.26 kcal mol^{-1} for the amphipathic MAP peptide. In absolute terms, these results indicate that, regardless of peptide class, single-peptide translocation across an intact bilayer is energetically unfavorable. In relative terms, the differences between our barriers and those reported by Catalina-Hernandez et al. are about 4% and 12%, respectively. While these differences are moderate, they do not alter the main conclusion: the membrane imposes a substantial energetic penalty that dominates peptide translocation.

To analyze the energetics of CPP translocation in more detail, conformations corresponding to intermediate states A, B and C (defined above) were extracted. State B matched the highest point on the PMF for both CPPs, confirming previous findings on other CPP/membrane pairs [33,36]. As a reference, a representative conformation of the isolated membrane against which to measure membrane disruptions was used.

Water ingress into the hydrophobic core and artifacts in the density of lipids around the CPP are symptomatic of CPP-induced membrane perturbations. To evaluate them, the water and cholesterol densities along the z axis (perpendicular to the membrane plane) were calculated (Fig. 2). For R9, it is noticeable that when the peptide penetrates the hydrophobic core, it drags the headgroups inward. This creates a defect in the membrane, which allows water to permeate it. However, the defect remains limited to the direct vicinity of the CPP: the formation of more extensive and long-lasting defects, such as barrel-stave or toroidal pores, require the collective action of multiple CPP molecules, triggered by higher peptide concentrations [79]. Furthermore, it is crucial that even these more elaborate defects remain transient: as noted by Allolio et al. [80], many CPPs are suspected to function by inducing transient local deformations or fusion pores that reclose rapidly. If these pores were long-lived or permanent, the peptides would cause massive depolarization and cytotoxicity, contradicting their known non-toxic profile at therapeutic concentrations. Cholesterol density is also perturbed, which is usually associated with the membrane's response to high bending [81,82]. In states A and B, it migrates from the lower leaflet and congregates around the peptide in the upper leaflet. Considering that the US windows are long enough to relax transient conformational stress, these defects can be considered meaningful, long-lived adaptations of the bilayer to the CPP which locally minimize the free energy penalty to permeation.

We now examine the evolution of the peptide-induced membrane curvature along the translocation pathway. Fig. 3 maps the local atomic curvatures on the membrane leaflets (which are used to compute the bending conformational coordinate Γ – see section 2.4 for details). Although it is the smallest peptide used in this study, R9 induced significant curvature in the membrane (Fig. 3). Polyarginines are known to form membrane defects, especially membrane bending, mainly because of the strong electrostatic effects between the arginine side chains and

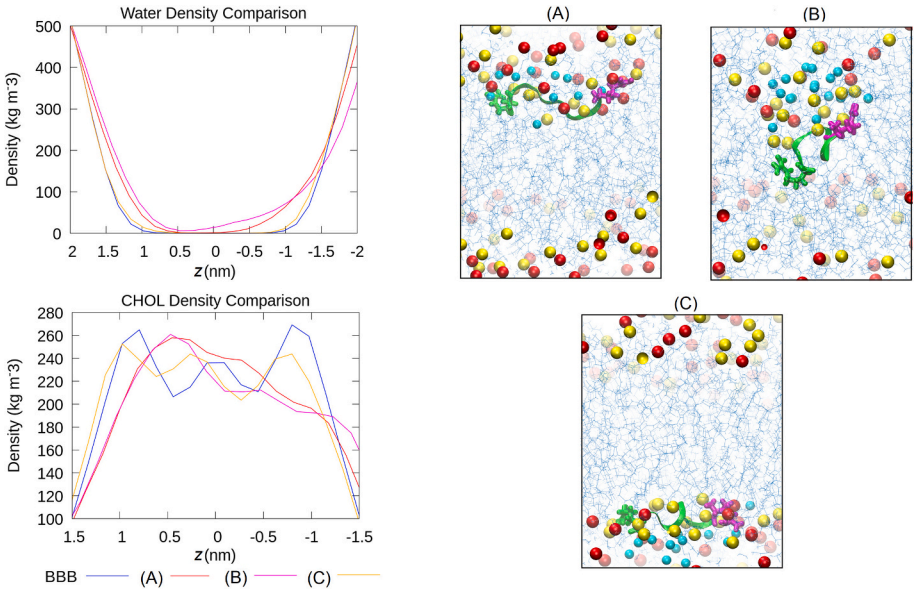

Fig. 2. Water and cholesterol density graphs and side view of the key R9 translocation intermediate states A, B and C (see text). The isolated membrane (BBB) is shown as reference. R9 is represented in green, with its N-terminus in magenta. Membrane features are colored as follows: hydrophobic core (blue lines), phosphorus from SA lipids (yellow spheres), phosphorus from other lipids (red spheres), and water (cyan spheres).

the phosphate group in lipids [60,83].

When closely examining the hydrogen bonding interactions involved in R9 translocation, it is possible to observe that SAPE appears as the main lipid partner interacting with R9, with an increasingly important role as the peptide moves through the membrane (Fig. 4). Density maps of SAPE PO4 in the x–y plane measured over the last quarter of the simulation confirm a dynamic behavior that follows the passage of CPP (Fig. 4). Other SA (1-stearoyl-2-arachidonoyl-sn-glycerol) lipids such as SAPI and SAPS also make durable contacts with the CPP. Such contacts can result in the dragging of the corresponding lipids across the membrane in the wake of the CPP. By shielding the CPP from the remainder of the membrane, these dragged lipids can mediate unfavorable interactions (in particular with the hydrophobic core), lowering the translocation free energy barrier. By following the CPP, they are very likely to end up in the opposite leaflet, from which other lipids might in turn depart to alleviate steric clashes. This can be thought of as an induced form of flip-flop, the leaflet exchange process that is known to facilitate peptide translocation [74,84–86]: in fact, in our simulations, only cholesterol was seen to feature spontaneous flip-flops; such events for all other lipids were exclusively due to the CPP translocation process. Lipids that change leaflets in the wake of the CPP can take a long while to reintegrate their original leaflet, resulting in durable changes to the membrane which explain the asymmetric nature of the obtained PMFs (also observed in other free energy studies [21,26] Similar peptide-mediated flip-flops have also very recently been reported by Cardenas and Elber for an anticancer peptide in a DOPC bilayer [87]. Our work shows that they are strongly lipid-specific and actively participate in the membrane-CPP recognition process.

Since the predominant role of SA lipids as CPP interaction partners cannot be solely attributed to their abundance in the membrane composition (POSM is even more represented), it is probably also related to the unique properties of their long unsaturated tails: these can adopt “angle-iron” [88] conformations which limit their effective lengths. This facilitates their travel toward the distal membrane leaflet, providing the CPP with a mobile “apolar cage” which assists its sliding through the hydrophobic core. It also favors the bending of the membrane by locally reducing its stiffness [88–92], again aiding CPP translocation. Finally, the lateral diffusion of the lipids is also increased, favoring their regrouping around the CPP. Thus, the complete mechanism can be conceived as a positive feedback loop between the CPP and the conformation and position of SA lipids within the membrane. Unfortunately, it is impossible to dissociate the quantitative effects on the translocation PMFs of direct interactions between CPPs and SA lipids from those of collective effects on membrane dynamics involving SA and other lipid types simultaneously: simulating a “chimeric” BBB depleted in SA lipids would thus not provide an unarguable reference to evaluate the free energy contribution of these lipids, despite their clear importance. Interestingly, the preferential interaction of the CPP with several distinct SA lipids suggests that the nature of the lipid chains is the main driver of CPP recognition, rather than the more traditionally invoked nature of lipid headgroup. This could be due to the MARTINI forcefield's limited ability to represent the chemical differences between headgroups (notably, the absence of an explicit hydrogen bonding term). However, since all SA lipid headgroups feature salt-bridging moieties, it is conceivable that a constant, nonspecific “background” population of salt bridges is preserved, shifting the specificity to the nature of the lipid chains. Previous studies have also observed that polyunsaturated fatty chains enhance headgroup flexibility [12] and are thus likely to modulate the recognition of the latter by peptides.

Coming back to our analysis of water and cholesterol density, we observed a different behavior for MPG. In comparison to R9, MPG did not significantly affect water density. The alteration in cholesterol distribution was less marked than for R9, despite a similar tendency to deplete the leaflet opposite to the CPP. This suggests a less damaging passage through the membrane for MPG (Fig. 5). Electrostatic anchoring of N-terminal and cationic residues emerges as a central determinant of MPG's membrane engagement and orientation (Fig. 6). Although lysine and arginine contribute to surface binding, arginine forms bidentate interactions with lipids, and therefore binds strongly [73]. This is evident in state B, where ARG25 maintains persistent contact with the upper leaflet, favoring orthogonal orientation. On the other hand, lysine side chains are often used to chemically link cargoes such as oligonucleotides, which MPG was originally designed to translocate [93]. Thus, in the presence of such a cargo, lysine engagement with the membrane may be reduced. Additionally, guanidinium bidentate interactions with lipid headgroups make it plausible that it can drag lipids inward, potentially facilitating local flip–flop events during translocation as seen earlier with SA lipids.

The reduced membrane stress associated with the crossing of MPG compared to R9 logically translates into fewer leaflet switch events

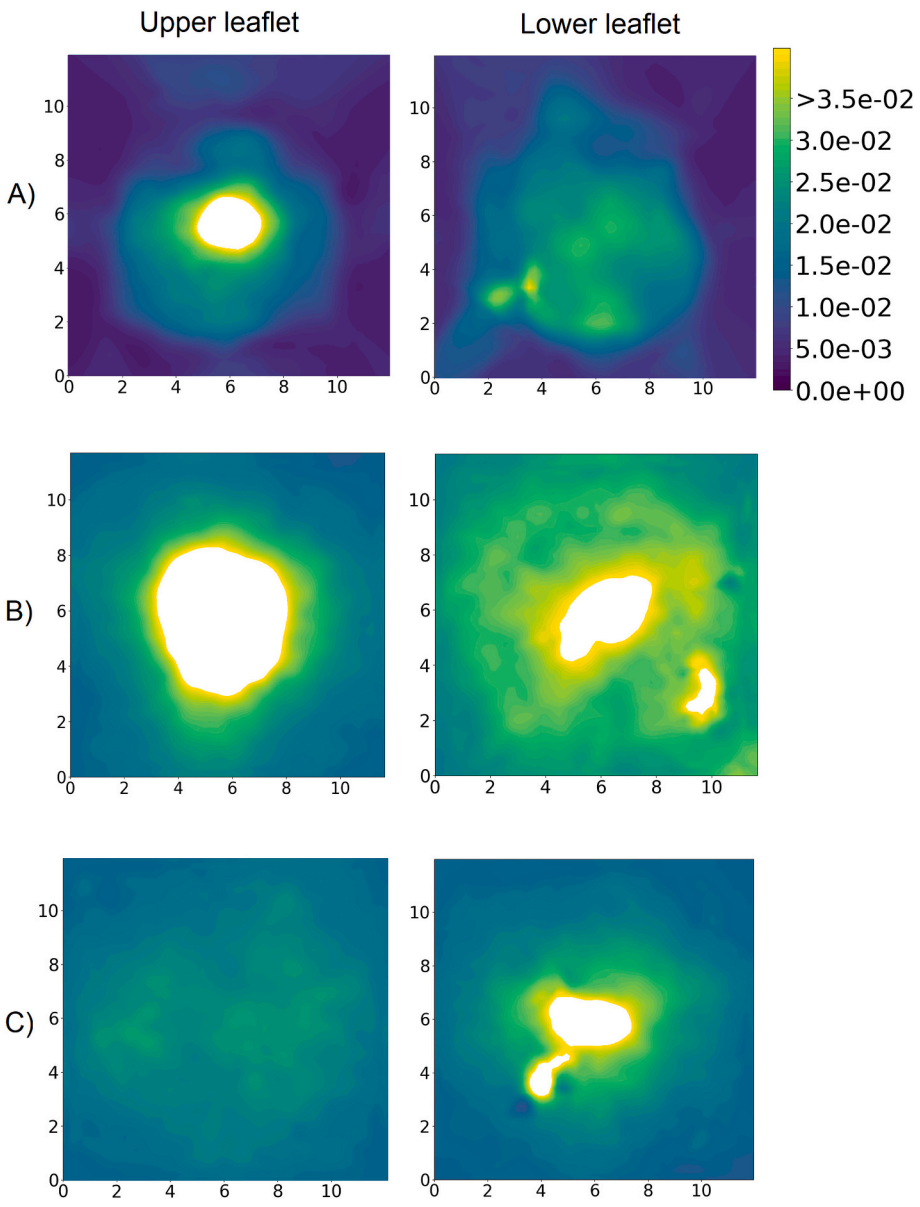

Fig. 3. Map of local atomic curvatures at the membrane headgroup beads of the upper and lower leaflets for the key R9 translocation intermediate states A, B and C (see text). The membrane is seen along the *z* axis, orthogonal to the membrane plane; dimensions along the *x* and *y* axes are expressed in nanometers. Lighter areas represent high curvature regions. All graphs share a common scale.

(Fig. S6). As for R9, these still mainly involve SA lipids, and not the equally highly represented POSM or SLPC. The synergy between SA leaflet switches, membrane bending and peptide translocation described for R9 also applies here. However, in contrast to R9 where all the lipids return to their original leaflet, MPG translocation triggers a persistent membrane asymmetry in which a few SAPC and SAPS from the inner leaflet remain in the outer one. This effect likely arises because MPG contains hydrophobic residues and reorientates when translocating. Such reorientation can cause a locally altered packing of the bilayer, creating a region where the bilayer becomes tighter on one side and more open in the other. Once accommodated in this region, bulky lipid headgroups may hinder their return of the original leaflet in the simulation time scale. However, caution must be taken in interpreting this data as in the presence of cargo, arginine and lysine residues triggering the translocation might not be available or exposed.

Analysis of local curvature, using the same scale and color scheme of R9's analysis confirms the milder effect of MPG on the membrane's integrity (Fig. 7). Despite this, and unlike R9, the curvature defects on the upper leaflet have not completely relaxed once MPG reaches the lower leaflet (state C). These observations can be explained by the fact that, unlike the much more compact and chemically homogeneous R9, MPG spans the entire membrane width during much of its translocation, favored by its amphipathic nature.

3.2. *Free energy as a function of membrane curvature*

Membrane bending is known to play an active role in the regulation of biological processes, via the reciprocal effects of membranes and proteins on each other's plasticity when both partners come into close vicinity [94]. In particular, arginine-rich CPPs are known to induce negative Gaussian curvature to facilitate the formation of transient membrane defects leading to translocation [95] In the “toroidal pore” or “water defect” models described in the literature, curvature generation is a prerequisite for reducing the energy penalty of charged peptide insertion [80,96] and the creation of pore defects [80,97]. We examine this effect for the studied CPPs, by monitoring how they affect the BBB's

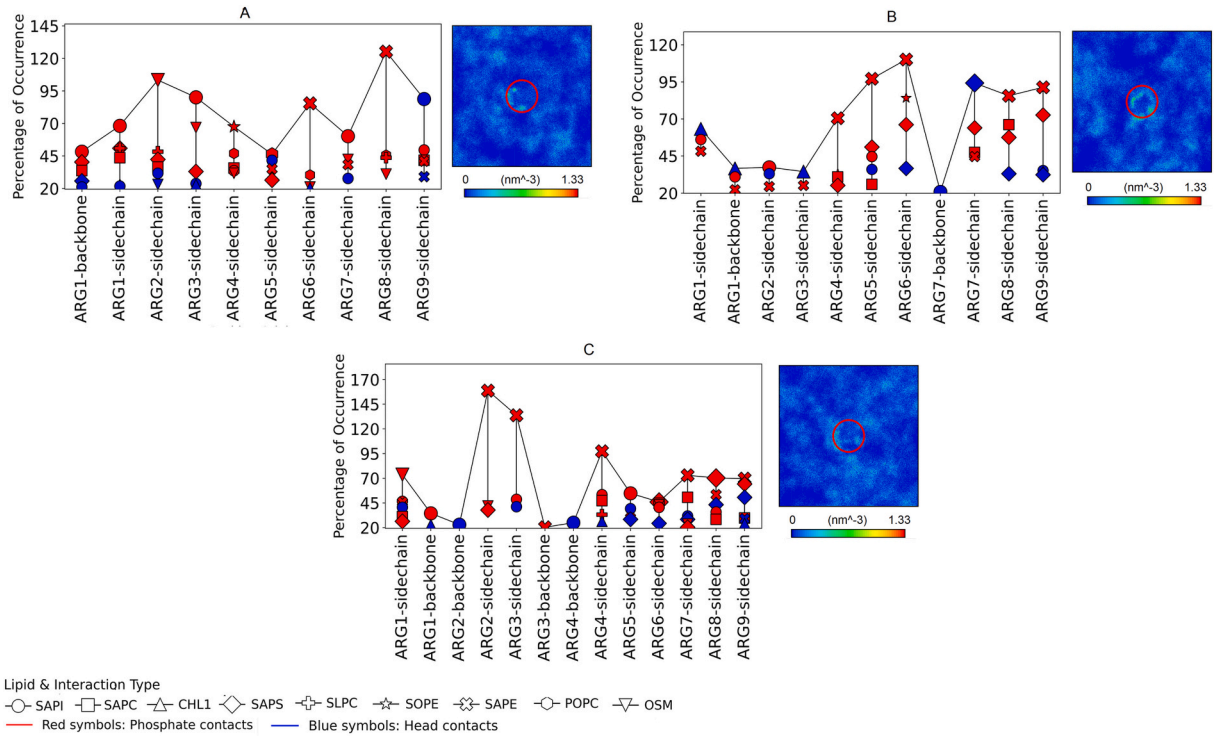

Fig. 4. Occurrence of hydrogen bonds between R9 and lipids and associated 2D map of SAPE PO4 density in the x–y plane, in the three key translocation intermediates A, B and C (see text). The red circle indicates the peptide's position. Only percentages greater than or equal to 20% are shown.

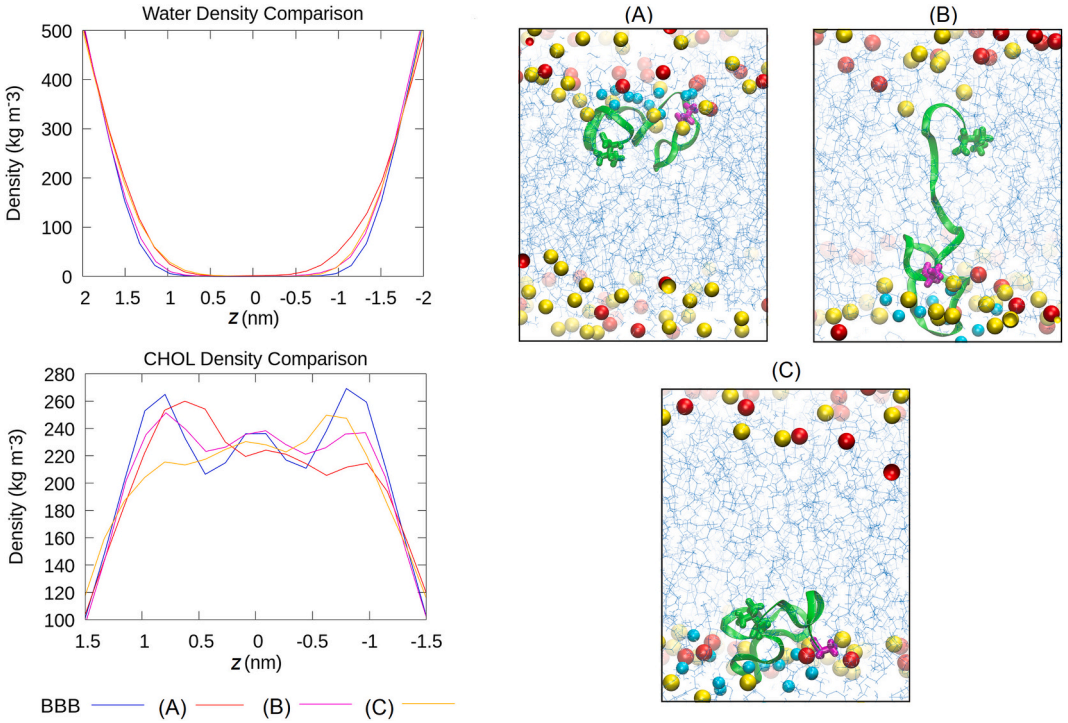

Fig. 5. Water and cholesterol density graphs and side view of the key MPG translocation intermediate states A, B and C (see text). MPG is represented in green, with its N-terminus in magenta. Membrane features are colored as follows: hydrophobic core (blue lines), phosphorus from SA lipids (yellow spheres), phosphorus from other lipids (red spheres), and water (cyan spheres).

bending propensity when adsorbed on its surface (intermediate state A defined above). Because of its high cholesterol and sphingomyelin content, dense packing and long acyl chains, the BBB is more rigid than simpler membranes. Estimates of bending moduli for model BBB bilayers range from 80 to 120 kBT, four to six times larger than the equivalent values for simple DOPC or POPC membranes [92,98,99]. Since membrane bending is instrumental to the translocation process, this rigidity contributes to the previously discussed low permeability

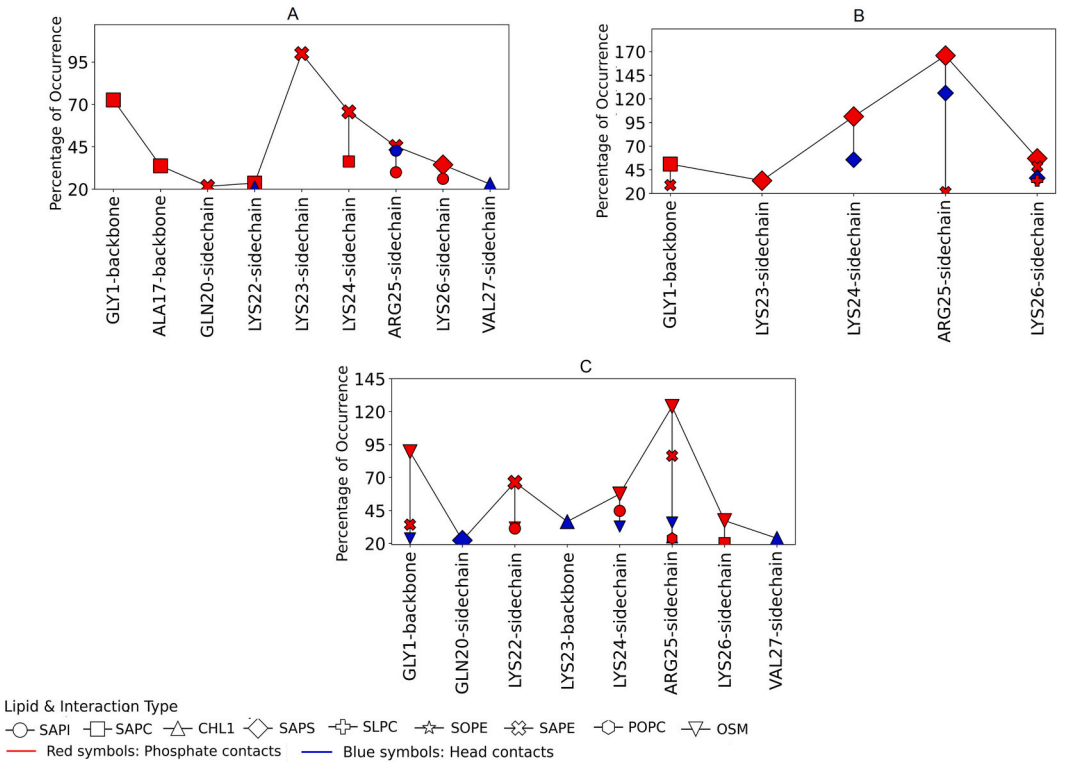

Fig. 6. Occurrence of hydrogen bonds between MPG and lipids in the three key translocation intermediates A, B and C (see text). Only percentages greater than or equal to 20% are shown.

and high free energy barriers. Hence, CPPs which are able to stabilize bent membrane conformations should be less penalized.

The free energy profiles obtained along the bending coordinate Γ (see Computational Methods) confirm that R9 favors and stabilizes high-curvature membrane conformations: the free energy minimum shifts from a flat membrane in the absence of R9 to a curved one in its presence, with curvature $\Gamma = 0.6$ (Fig. 8, left). This finding supports previous observations that one of the mechanisms of arginine-rich CPPs translocation involves inducing membrane curvature [83]. In addition, the slope of the PMF around the minimum is markedly lower in the presence of BBB, signaling an enhanced membrane plasticity which should entropically favor translocation. Interestingly, the membrane deformations induced in our simulations cause the bending of lipid headgroups to interact with the peptide (Fig. 8). This is perfectly compatible with the initiation of a toroidal pore in which the reorientation of phosphate groups allows the insertion of the arginines inside the membrane [12].

On the other hand, the presence of MPG on the membrane surface has a much weaker effect on curvature: conformations with moderate curvatures ($\Gamma \sim 0.3$ in Fig. 8, right) are slightly favored, but the flat membrane remains the preferred structure. $\Gamma = 0.45$ features an intersection point, suggesting that more bent structures are unfavorable, probably due to steric and electrostatic constraints imposed by the peptide. Furthermore, the slope of the PMF around the minimum is not affected by the presence of the CPP, which seemingly does not alleviate the BBB's rigidity. Because the crossings of the BBB by R9 and MPG both involve membrane bending, the stabilization of bent conformations by R9 is a facilitating factor for the translocation of this peptide that does not exist for MPG. Presumably, it contributes to bringing the free energy barrier to R9 translocation, otherwise higher, within range of that of MPG. However, quantifying this effect would require 2D enhanced sampling simulations, introducing bias along both the translocation and bending conformational coordinates; unfortunately, these have a prohibitive computational cost since all possible values of the second coordinate must be fully equilibrated at every value of the first. In any case, the effect is not sufficient to invert the order of free energy barriers between both CPPs. Additionally, even though MPG does not actively promote bending, the associated barrier is small (around 5 kcal mol^{-1}, see Fig. 8); paying such a small price would still be a worthwhile tradeoff to alleviate unfavorable steric and electrostatic interactions that would otherwise occur for the MPG in a flat membrane.

3.3. *Influence of CPP secondary structure*

Molecular compactness has a pivotal role in membrane translocation, as distinct secondary structures can significantly modulate a peptide's capacity to penetrate lipid bilayers [100]. To assess the influence of peptide folding on the translocation process, Rg was used as a CV in WTM simulations (see Computational Methods) which were performed on 2 different intermediate states: the first few contacts between CPP and BBB (called state A0 from here on) and the previously defined intermediate state A (corresponding to the adsorbed CPP). Analogous WTM simulations were also performed on the CPP in bulk water and in octane, as references and to mimic the conditions encountered by the CPP far from the membrane and within the membrane core, respectively. The results show that R9 in water is unstructured, with accessible Rg ranging from 0.6 nm to 1.0 nm but a preference for the 0.85–1.0 nm range due to a moderate kinetic barrier around 0.7 nm. In the presence of the membrane, whether near or fully adsorbed onto its surface, the span of Rg values does not drastically change, but the more folded conformations ($Rg < 0.8$ nm) tend to be stabilized and the kinetic barrier disappears. This indicates that the membrane enhances the peptide's conformational freedom and therefore facilitates translocation from an energetic perspective: if rigidification occurred at this stage, it would make translocation entropically less favorable. In octane, such a rigidification is indeed observed and only the folded structure remains statistically relevant (which is expected for a polar CPP in a purely hydrophobic environment). Such conditions can be encountered in the membrane core; however, by this point the peptide has already crossed the principal free energy barrier (intermediate B discussed above), so

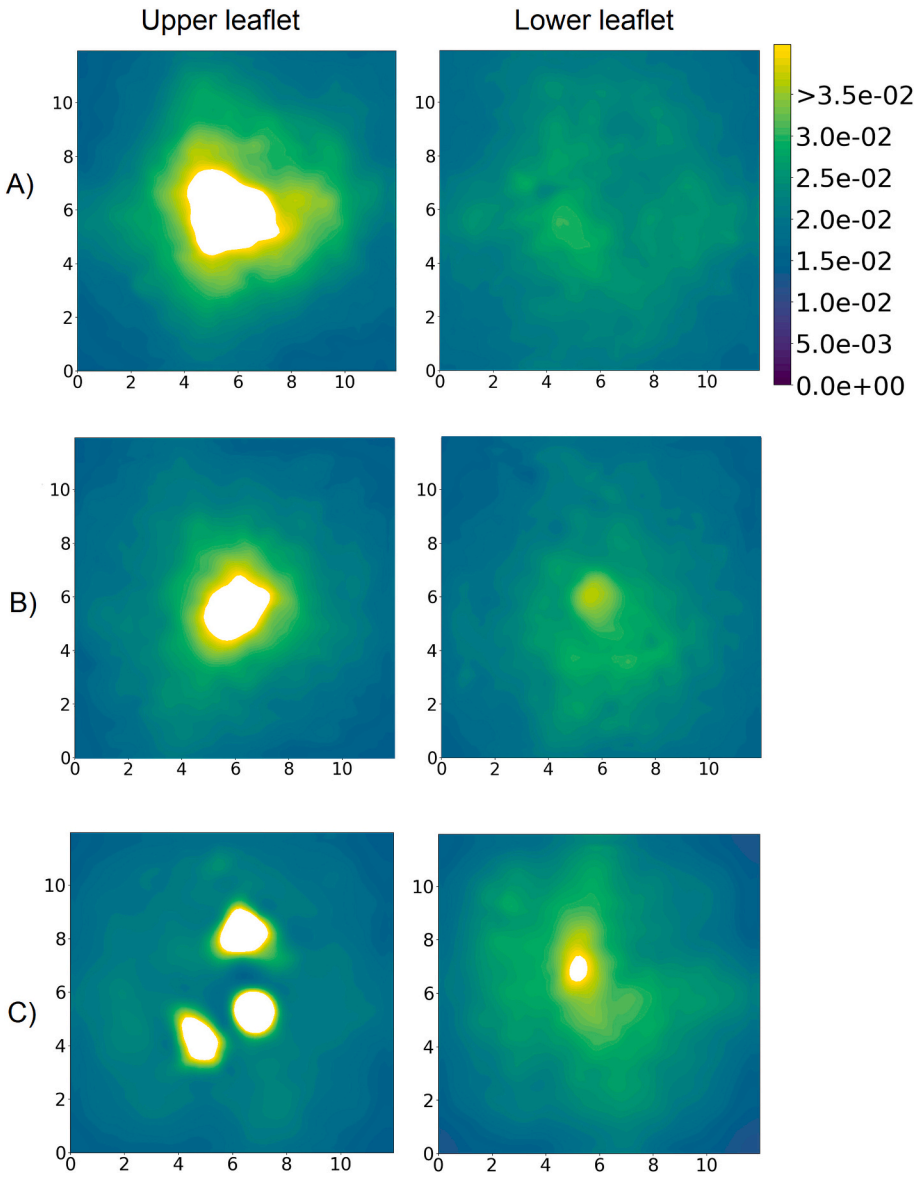

Fig. 7. Map of local atomic curvatures at the membrane headgroup beads of the upper and lower leaflets for the key MPG translocation intermediate states A, B and C (see text). The membrane is seen along the *z* axis, orthogonal to the membrane plane; dimensions along the *x* and *y* axes are expressed in nanometers. Lighter areas represent high curvature regions. Lighter areas represent high curvature regions. All graphs share a common scale.

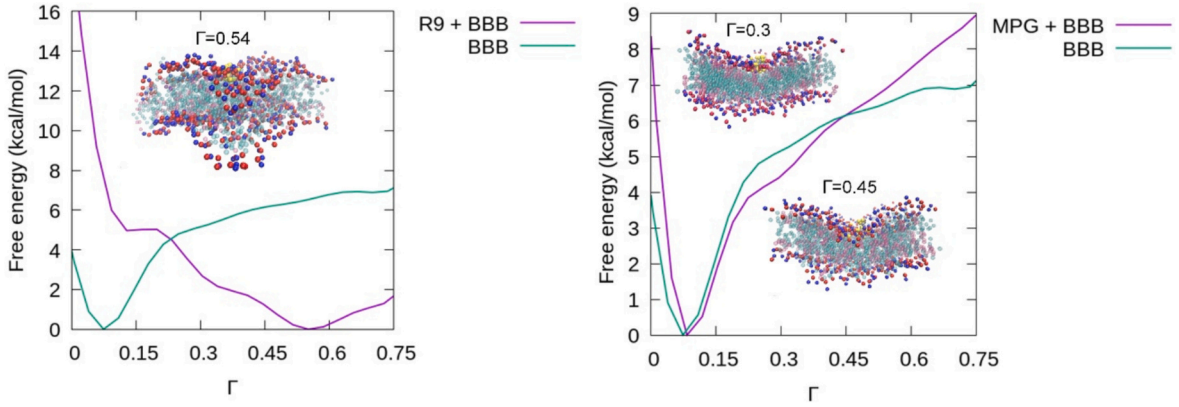

Fig. 8. Comparison of bending free energy profiles between the membrane alone (cyan) and in the presence of R9 (left) and MPG (right) (purple). Membrane components in the coarse-grained representation are colored as follows: hydrophobic core (cyan spheres), phosphate- and oxygen-containing functional groups (red spheres), and nitrogen-containing functional groups (blue).

this effect does not alter the overall permeation energetics.

Hydrogen-bond analysis of state A0 shows that R9 interacts with the membrane primarily through its N-terminus (Fig. 9 and Fig. S7), whereas in state A all arginine side chains form persistent hydrogen bonds with lipid headgroups, ensuring anchoring of the peptide at the surface (Fig. 9 and Fig. S8). The persistence of arginine bidentate interactions has been highlighted in the literature as a key factor underlying the effectiveness of arginine-rich CPPs in membrane translocation [101–103], since stable anchoring at the surface is considered a critical first step [18]. DSSP analyses confirm that R9 is predominantly unstructured in all the intermediate states considered, in line with experimental observations [104] although loops change to slightly more rigid turns and bends in octane (Fig. S9-S11).

The results for MPG show that compact conformations are favored across environments, with the main difference lying in the energy cost for adopting extended configurations (Fig. 10). In water, the peptide tends to fold to minimize the exposure of hydrophobic residues to the polar solvent: extended conformations are penalized by ~20 kcal mol^{-1}. When the peptide is near the membrane surface (A0), higher Rg becomes more easily accessible because the membrane provides a thermodynamically favorable interface where side chains can interact, thereby reducing the energetic penalty to unfolding. This partial unfolding of MPG is accompanied by a reorientation of the peptide: in the folded state, the C-terminus points toward the membrane, with LYS24 and ARG25 playing an essential role in lipid interaction (Fig. 10 and Fig. S12 for details), while in extended states the N-terminus maintains membrane contact (Fig. S12). Indeed, ARG25 could be the main responsible for the delivery of MPG to the surface by electrostatic attraction to the negatively charged lipids. A similar reorientation behavior was also reported in other CPPs with C-terminal lysine residues. This trend can be explained by the hydrophilic nature of lysine, which tends to orient toward the aqueous phase [105]. When the peptide is adsorbed in the membrane (A), folded conformations are strongly favored by electrostatic interactions involving GLY1, LYS22–23, ARG25 and LYS26, but also by steric restriction (Fig. 10 and Fig. S13 for details).

It should be kept in mind that these results correspond to the free form of MPG, in which the charged C-terminus is free to interact with the membrane. As mentioned in section 3.1, in the functional peptide, these charged residues (especially LYS) serve as an anchor to cargos, meaning that their availability for membrane interaction would be reduced. However, our results also capture the involvement of the N-terminus, which is coherent with experimental studies that have identified this region as the main driver of the initial membrane contact [93]. This agreement with experimental data further supports the effectiveness of simulations in recovering mechanistic features of CPP–membrane interactions.

In octane, the exposure of hydrophilic residues to the hydrophobic medium imposes an even higher energetic penalty for extended conformations. Interestingly, MPG consistently favors compact states across intermediates, suggesting that the dominant barrier to translocation is enthalpic rather than entropic, at least when considering the monomer without the cargo. Together, the results suggest that MPG's mostly hydrophobic nature enables a less disruptive passage through the membrane; and that its translocation is less entropically demanding compared to R9, accounting for its slightly lower free energy barrier for translocation. Nevertheless, the enthalpic cost for crossing the hydrophobic core still imposes a significant barrier. It should be noted that the HIV-1 Fusion Domain, constituting the N-terminal portion of MPG, has been shown to form a well-defined alpha helix which transition to a beta-like elongated structure in the presence of increasing concentrations of cholesterol [106].

Secondary structure analysis reveals that MPG remains largely disordered in all states, albeit to a lesser extent than R9 (Fig. S14–16). In water, this result is consistent with experimental observations [104], while the behavior in the membrane may seem controversial, given that this peptide is expected to assume more defined secondary structures. Electrostatic interactions play a central role in the structural modulation of peptides on the membrane. For instance, it is documented that some CPPs that can form β-sheet structures in fully anionic membranes tend to adopt random coil structures in membranes with more physiologically representative compositions [104]. This observation suggests that the absence of defined secondary structures may be attributable to the lack of a full negative surface charge that might be required to stabilize more ordered peptide conformations. Collectively, these findings indicate that under these conditions MPG's association with the membrane is driven more by electrostatic interactions with lipids than by the stabilization of specific secondary structures. However, these analyses should be interpreted with caution due to their inherent limitations. Weakly structured peptides can adopt a wide range of functionally similar conformations, with only slight differences in compactness, making thorough sampling challenging. Furthermore, despite the validation and replication of experimental trends by the GoMartini model [56], its representation of

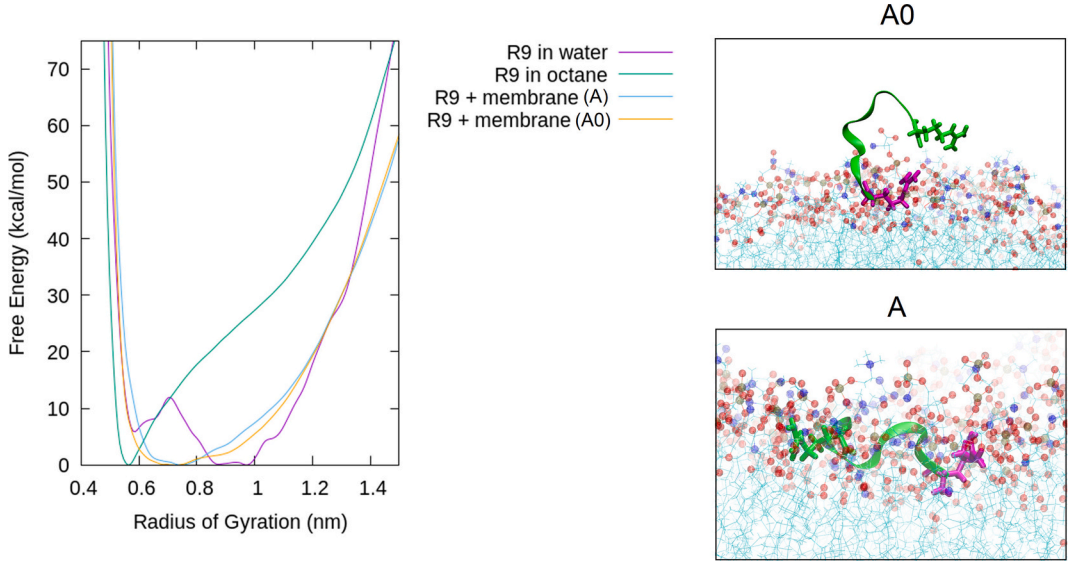

Fig. 9. Left: free energy as a function of Rg for R9 in different conditions. Right: representative conformations of the free energy minima for states A0 and A in the presence of the membrane. The peptide is represented in green, with its N-terminus in magenta. Membrane features are colored as follows: hydrophobic core (cyan lines), oxygen (red spheres), phosphorus (dark tan spheres), and nitrogen (blue spheres).

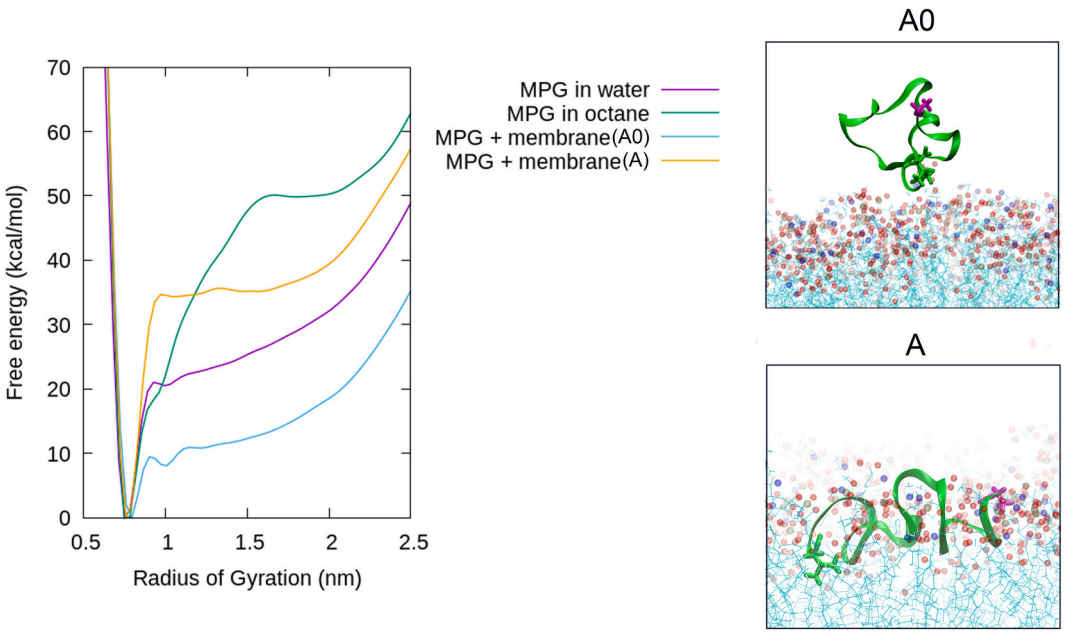

Fig. 10. Left: free energy as a function of Rg for MPG in different conditions. Right: representative conformations of the free energy minima for states A0 and A in the presence of the membrane. The peptide is represented in purple, with its N-terminus in magenta and C-terminus in green. Membrane features are colored as follows: hydrophobic core (cyan lines), oxygen (red spheres), phosphorus (dark tan spheres), and nitrogen (blue spheres).

folding and unfolding free energy landscapes remains approximate, which might have more consequences for small peptides than for larger globular proteins. However, when comparing different systems relative to one another, we expect possible artifacts to cancel out, preserving the overall message.

Finally, it is important to acknowledge the limitations of this study. The literature shows that CPPs can use multiple translocation mechanisms, and that transitions between them can be triggered by peptide concentration [13,107]. At higher concentrations, CPPs may switch to less energetically costly and cooperative mechanisms [108] that were not considered here. This is particularly true for the case of MPG peptide, in which aggregation around the cargo forms a protective hydrophobic cage allowing the translocation through the hydrophobic core of the membrane [108]. Although simulating a single peptide is a crucial step toward understanding CPP translocation, allowing us to identify key residues involved in membrane interactions and to obtain a thermodynamic perspective, the absence of concentration effects remains a limitation that warrants further investigation.

4. Conclusions

In the present study, we combined coarse-grained molecular dynamics simulations and enhanced sampling techniques to describe the translocation mechanism of two well-known CPPs (R9 and MPG) in a realistic membrane model. With this coarse-grained approach, we trade the explicit description of atomic interactions against the possibility to gain access to long timescales, compatible with large-scale membrane rearrangements and crucial for the accurate evaluation of free energy barriers. Our work is a valuable addition to the growing number of applications of these methods to membrane translocation problems. While R9 penetration causes significant disturbances in the membrane, MPG follows a less disruptive interaction pathway despite its larger size. Nevertheless, despite inducing distinct patterns of membrane perturbation, both peptides face large resistance when entering the membrane. This behavior is consistent with the complexity of the BBB and its specific composition, suggesting that the resistance appears to be largely governed by membrane composition rather than solely by the CPP's chemical class (cationic vs. amphipathic). Unfortunately, evaluating the role of specific membrane components is made difficult by the existence of collective effects in such complex multi-component membranes. However, this does not diminish the importance of primary sequence design. Rather, it redefines the role of specific residues: instead of merely "lowering" the barrier, the amino acids dictate the mechanistic pathway, and the frequency of translocation attempts via surface recruitment. For highly restrictive membranes like the BBB, this implies that design efforts should prioritize maximizing membrane residency time and structural adaptability to satisfy the bilayer's inherent thermodynamic constraints. Additionally, the high barrier also suggests that translocation might be facilitated for alternative uptake routes or other system conditions.

The simulations also suggest that both peptides initiate membrane interactions via their N-terminus suggesting that preserving this region is important for peptide insertion. Additionally, even in MPG, arginine was shown to be pivotal for membrane binding. Nevertheless, studying free peptides allowed us to highlight sequence-dependent features that govern their interaction with membranes and can modulate their capacity as CPPs. Our study also highlights the strikingly different effects of the CPPs on membrane curvature, which hints at an underlying indirect recognition mechanism between CPP and membrane. Notably, our results reveal that both CPPs selectively recruit highly unsaturated lipids (SAPE, SAPI, SAPS) during translocation, which redistribute between both leaflets in the wake of the CPP's passage via induced flip-flop events. This suggests that curvature-adaptative lipid species actively participate in alleviating the mechanical stresses induced by peptides. Finally, we revealed the remarkable role of the membrane in stabilizing CPP conformations that are disfavored in bulk water (folded for R9, unfolded for MPG), thereby reducing the entropic penalty to translocation. We hope that our results may pave the way for a better fundamental understanding of complex CPP-BBB interactions, paramount for the design of optimized CPPs to carry therapeutic cargos across the BBB.

CRediT authorship contribution statement

Cintia Emi Yanaguibashi Leal: Writing – original draft, Visualization, Investigation. **Nicola D'Amelio:** Writing – review & editing,

Supervision, Conceptualization. **Benjamin Bouvier:** Writing – review & editing, Supervision, Software, Methodology, Conceptualization.

Declaration of competing interest

The authors declare that they have no competing interests with individuals or organizations that could influence this work.

Acknowledgements

The calculations presented herein were performed using HPC resources from the MatriCS computing platform of Université de Picardie - Jules Verne, Amiens, France.

Appendix A. Supplementary data

Supplementary data to this article can be found online at https://doi.org/10.1016/j.bbamem.2026.184525.

Data availability

Data will be made available on request.

References

[1] J.D. Steinmetz, K.M. Seeher, N. Schiess, E. Nichols, B. Cao, C. Servili, et al., Global, regional, and national burden of disorders affecting the nervous system, 1990–2021: a systematic analysis for the global burden of disease study 2021, The Lancet Neurology. 23 (4) (2024) 344–381, https://doi.org/10.1016/S1474-4422(24)00038-3. Apr.

[2] N.J. Abbott, I.A. Romero, Transporting therapeutics across the blood-brain barrier, Mol. Med. Today 2 (3) (1996) 106–113, https://doi.org/10.1016/1357-4310(96)88720-X. Mar.

[3] J.H. Pedder, A.M. Sonabend, M.D. Cearns, B.D. Michael, R. Zakaria, A. B. Heimberger, et al., Crossing the blood–brain barrier: emerging therapeutic strategies for neurological disease, The Lancet Neurology. 24 (3) (2025) 246–260, https://doi.org/10.1016/S1474-4422(24)00476-9. Mar.

[4] D. Wu, Q. Chen, X. Chen, F. Han, Z. Chen, Y. Wang, The blood–brain barrier: structure, regulation and drug delivery, Sig Transduct Target Ther. 8 (1) (2023) 217, https://doi.org/10.1038/s41392-023-01481-w. May 25.

[5] S.M. Stamatovic, A.M. Johnson, R.F. Keep, A.V. Andjelkovic, Junctional proteins of the blood-brain barrier: new insights into function and dysfunction, Tissue Barriers. 4 (1) (2016), https://doi.org/10.1080/21688370.2016.1154641 PubMed PMID: 27141427; PubMed Central PMCID: PMC4836471 e1154641. Feb 26.

[6] J. Rustenhoven, D. Jansson, L.C. Smyth, M. Dragunow, Brain Pericytes as mediators of Neuroinflammation, Trends Pharmacol. Sci. 38 (3) (2017) 291–304, https://doi.org/10.1016/j.tips.2016.12.001. Mar.

[7] L.N. Zamproni, B. Gökçe, J. Venckute Larsson, A. Ceballos-Torres, M. Gram, M. A. Porcionatto, et al., Unraveling the influence of astrocytes on endothelial cell transcription: towards understanding blood-brain barrier *in vitro* models' dynamics, Brain Res. Bull. 224 (2025), https://doi.org/10.1016/j.brainresbull.2025.111328, 111328. May 1.

[8] A. Verkhratsky, A. Pivoriūnas, Astroglia support, regulate and reinforce brain barriers, Neurobiol. Dis. 1 (179) (2023), https://doi.org/10.1016/j.nbd.2023.106054, 106054. Apr.

[9] Thomsen MS, Routhe LJ, Moos T. The vascular basement membrane in the healthy and pathological brain. J. Cereb. Blood Flow Metab. 2017Oct 1;37(10): 3300–17. doi:https://doi.org/10.1177/0271678X17722436.

[10] B. Oller-Salvia, M. Sánchez-Navarro, E. Giralt, M. Teixidó, Blood–brain barrier shuttle peptides: an emerging paradigm for brain delivery, Chem. Soc. Rev. 45 (17) (2016) 4690–4707, https://doi.org/10.1039/C6CS00076B. Aug 22.

[11] S.D. Campbell, K.J. Regina, E.D. Kharasch, Significance of lipid composition in a blood-brain barrier-mimetic PAMPA assay, J. Biomol. Screen. 19 (3) (2014) 437–444, https://doi.org/10.1177/1087057113497981 PubMed PMID: 23945876; PubMed Central PMCID: PMC4078735. Mar.

[12] H.D. Herce, A.E. Garcia, J. Litt, R.S. Kane, P. Martin, N. Enrique, et al., Arginine-rich peptides destabilize the plasma membrane, consistent with a pore formation translocation mechanism of cell-penetrating peptides, Biophys. J. 97 (7) (2009) 1917–1925, https://doi.org/10.1016/j.bpj.2009.05.066. Oct 7.

[13] A. Gori, G. Lodigiani, S.G. Colombarolli, G. Bergamaschi, A. Vitali, Cell penetrating peptides: classification, mechanisms, methods of study, and applications, ChemMedChem 18 (17) (2023), https://doi.org/10.1002/cmdc.202300236 e202300236.

[14] I. Rusiecka, J. Ruczyński, A. Kozłowska, E. Backtrog, P. Mucha, I. Kocić, et al., TP10-dopamine conjugate as a potential therapeutic agent in the treatment of Parkinson's disease, Bioconjug. Chem. 30 (3) (2019) 760–774, https://doi.org/10.1021/acs.bioconjchem.8b00894. Mar 20.

[15] K.S. Rao, M.K. Reddy, J.L. Horning, V. Labhasetwar, TAT-conjugated nanoparticles for the CNS delivery of anti-HIV drugs, Biomaterials 29 (33) (2008) 4429–4438, https://doi.org/10.1016/j.biomaterials.2008.08.004. Nov.

[16] P.C. Chiu, H.C. Liou, T.Y. Ling, L.J. Shen, Development of a neuroprotective erythropoietin modified with a novel carrier for the blood-brain barrier, Neurotherapeutics 17 (3) (2020) 1184–1196, https://doi.org/10.1007/s13311-020-00845-2. Jul.

[17] D.M. Copolovici, K. Langel, E. Eriste, Ü. Langel, Cell-penetrating peptides: design, synthesis, and applications, ACS Nano 8 (3) (2014) 1972–1994, https://doi.org/10.1021/nn4057269. Mar 25.

[18] S. Yesylevskyy, S.J. Marrink, A.E. Mark, Alternative mechanisms for the interaction of the cell-penetrating peptides Penetratin and the TAT peptide with lipid bilayers, Biophys. J. 97 (1) (2009) 40–49, https://doi.org/10.1016/j.bpj.2009.03.059. Jul 8.

[19] K.P. Santo, M.L. Berkowitz, Difference between Magainin-2 and Melittin assemblies in phosphatidylcholine bilayers: results from coarse-grained simulations, J. Phys. Chem. B 116 (9) (2012) 3021–3030, https://doi.org/10.1021/jp212018f. Mar 8.

[20] D.P. Tran, S. Tada, A. Yumoto, A. Kitao, Y. Ito, T. Uzawa, et al., Using molecular dynamics simulations to prioritize and understand AI-generated cell penetrating peptides, Sci. Rep. 11 (1) (2021) 10630, https://doi.org/10.1038/s41598-021-90245-z. May 20.

[21] J. Gimenez-Dejoz, K. Numata, Molecular dynamics study of the internalization of cell-penetrating peptides containing unnatural amino acids across membranes, Nanoscale Advances. 4 (2) (2022) 397–407, https://doi.org/10.1039/D1NA00674F.

[22] Zwier MC, Chong LT. Reaching biological timescales with all-atom molecular dynamics simulations. Curr. Opin. Pharmacol. 2010Dec 1;Endocrine and metabolic diseases/New technologies - the importance of protein dynamics10(6): 745–52. doi:https://doi.org/10.1016/j.coph.2010.09.008.

[23] G. Drin, M. Mazel, P. Clair, D. Mathieu, M. Kaczorek, J. Temsamani, Physico-chemical requirements for cellular uptake of pAntp peptide, Eur. J. Biochem. 268 (5) (2001) 1304–1314, https://doi.org/10.1046/j.1432-1327.2001.01997.x.

[24] J.N. Onuchic, Z. Luthey-Schulten, P.G. Wolynes, THEORY OF PROTEIN FOLDING: the energy landscape perspective, Annu. Rev. Phys. Chem. 48 (1) (1997) 545–600, https://doi.org/10.1146/annurev.physchem.48.1.545. Oct.

[25] Bennett AL, Cranford KN, Bates AL, Sabatini CR, Lee HS. A molecular dynamics study of cell-penetrating peptide transportan-10 (TP10): binding, folding and insertion to transmembrane state in zwitterionic membrane. Biochim. Biophys. Acta Biomembr. 2024Jan 1;1866(1):184218. doi:https://doi.org/10.1016/j.bbamem.2023.184218.

[26] E. Catalina-Hernandez, M. Aguilella-Arzo, A. Peralvarez-Marin, M. Lopez-Martin, Computational insights into membrane disruption by cell-penetrating peptides, J. Chem. Inf. Model. 65 (3) (2025) 1549–1559, https://doi.org/10.1021/acs.jcim.4c01940. Feb 10.

[27] M. Pourmousa, J. Wong-ekkabut, M. Patra, M. Karttunen, Molecular dynamic studies of Transportan interacting with a DPPC lipid bilayer, J. Phys. Chem. B 117 (1) (2013) 230–241, https://doi.org/10.1021/jp310255r. Jan 10.

[28] Valsson O, Tiwary P, Parrinello M. Enhancing important fluctuations: rare events and metadynamics from a conceptual viewpoint. Annu. Rev. Phys. Chem. 2016May 27;67(Volume 67, 2016):159–84. doi:https://doi.org/10.1146/annurev-physchem-040215-112229.

[29] H. Fu, H. Bian, X. Shao, W. Cai, Collective variable-based enhanced sampling: from human learning to machine learning, J. Phys. Chem. Lett. 15 (6) (2024) 1774–1783, https://doi.org/10.1021/acs.jpclett.3c03542. Feb 15.

[30] S.J. Marrink, H.J. Risselada, S. Yefimov, D.P. Tieleman, A.H. De Vries, The MARTINI force field: coarse grained model for biomolecular simulations, J. Phys. Chem. B 111 (27) (2007) 7812–7824, https://doi.org/10.1021/jp071097f. Jul 1.

[31] I. Kabelka, R. Brožek, R. Vácha, Selecting collective variables and free-energy methods for peptide translocation across membranes, J. Chem. Inf. Model. 61 (2) (2021) 819–830, https://doi.org/10.1021/acs.jcim.0c01312. Feb 22.

[32] E.N. Frigini, R.D. Porasso, T. Beke-Somfai, J.J. López Cascales, R.D. Enriz, S. Pantano, The mechanism of antimicrobial small-cationic peptides from coarse-grained simulations, J. Chem. Inf. Model. 63 (21) (2023) 6877–6889, https://doi.org/10.1021/acs.jcim.3c01348. Nov 13.

[33] B.T. Kumara, N.K. Wijesiri, P.V.G.M. Rathnayake, R.J.K.U. Ranatunga, A re-evaluation of the free energy profiles for cell-penetrating peptides across DOPC membranes, Int. J. Pept. Res. Ther. 27 (4) (2021) 2931–2943, https://doi.org/10.1007/s10989-021-10301-0. Dec 1.

[34] B. Wang, J. Zhang, Y. Zhang, Z. Mao, N. Lu, Q.H. Liu, The penetration of a charged peptide across a membrane under an external electric field: a coarse-grained molecular dynamics simulation, RSC Adv. 8 (72) (2018) 41517–41525, https://doi.org/10.1039/C8RA07654E. Dec 7.

[35] Y. Wang, E. Gallagher, C. Jorgensen, E.P. Troendle, D. Hu, P.C. Searson, et al., An experimentally validated approach to calculate the blood-brain barrier permeability of small molecules, Sci. Rep. 9 (1) (2019) 6117, https://doi.org/10.1038/s41598-019-42272-0. Apr 16.

[36] F. Her Choong, Yap B. Keat, Cell-penetrating peptides: correlation between peptide-lipid interaction and penetration efficiency, ChemPhysChem 22 (5) (2021) 493–498, https://doi.org/10.1002/cphc.202000873. Mar 3.

[37] K. Huang, A.E. García, Free energy of translocating an arginine-rich cell-penetrating peptide across a lipid bilayer suggests pore formation, Biophys. J. 104 (2) (2013) 412–420, https://doi.org/10.1016/j.bpj.2012.10.027. Jan 22.

[38] G. Grasso, S. Muscat, M. Rebella, U. Morbiducci, A. Audenino, A. Danani, et al., Cell penetrating peptide modulation of membrane biomechanics by molecular

dynamics, J. Biomech. 73 (2018) 137–144, https://doi.org/10.1016/j.jbiomech.2018.03.036. May.
[39] L. Monticelli, S.K. Kandasamy, X. Periole, R.G. Larson, D.P. Tieleman, S. J. Marrink, The MARTINI coarse-grained force field: extension to proteins, J. Chem. Theory Comput. 4 (5) (2008) 819–834, https://doi.org/10.1021/ct700324x. May.
[40] K. Melikov, L.V. Chernomordik, Arginine-rich cell penetrating peptides: from endosomal uptake to nuclear delivery, Cell. Mol. Life Sci. 62 (23) (2005) 2739–2749, https://doi.org/10.1007/s00018-005-5293-y. Dec.
[41] S. Deshayes, M. Morris, F. Heitz, G. Divita, Delivery of proteins and nucleic acids using a non-covalent peptide-based strategy, Adv. Drug Deliv. Rev. 60 (4–5) (2008) 537–547, https://doi.org/10.1016/j.addr.2007.09.005. Mar.
[42] F. Ramos-Martín, T. Annaval, S. Buchoux, C. Sarazin, N. D'Amelio, ADAPTABLE: a comprehensive web platform of antimicrobial peptides tailored to the user's research, Life Sci Alliance. 2 (6) (2019), https://doi.org/10.26508/lsa.201900512 e201900512. Nov 18.
[43] B.R. Brooks, C.L. Brooks III, A.D. Mackerell Jr., L. Nilsson, R.J. Petrella, B. Roux, et al., CHARMM: the biomolecular simulation program, J. Comput. Chem. 30 (10) (2009) 1545–1614, https://doi.org/10.1002/jcc.21287.
[44] J. Lee, X. Cheng, J.M. Swails, M.S. Yeom, P.K. Eastman, J.A. Lemkul, et al., CHARMM-GUI input generator for NAMD, GROMACS, AMBER, OpenMM, and CHARMM/OpenMM simulations using the CHARMM36 additive force field, J. Chem. Theory Comput. 12 (1) (2016) 405–413, https://doi.org/10.1021/acs.jctc.5b00935. Jan 12.
[45] S. Jo, T. Kim, V.G. Iyer, W. Im, CHARMM-GUI: a web-based graphical user interface for CHARMM, J. Comput. Chem. 29 (11) (2008) 1859–1865, https://doi.org/10.1002/jcc.20945.
[46] P.C.T. Souza, R. Alessandri, J. Barnoud, S. Thallmair, I. Faustino, F. Grünewald, et al., Martini 3: a general purpose force field for coarse-grained molecular dynamics, Nat. Methods 18 (4) (2021) 382–388, https://doi.org/10.1038/s41592-021-01098-3. Apr.
[47] J.K. Spinti, F. Neiva Nunes, M.N. Melo, Room for improvement in the initial martini 3 parameterization of peptide interactions, Chem. Phys. Lett. 16 (819) (2023), https://doi.org/10.1016/j.cplett.2023.140436, 140436. May.
[50] G.A. Tribello, M. Bonomi, D. Branduardi, C. Camilloni, G. Bussi, PLUMED 2: new feathers for an old bird, Comput. Phys. Commun. 185 (2) (2014) 604–613, https://doi.org/10.1016/j.cpc.2013.09.018. Feb.
[51] G.M. Torrie, J.P. Valleau, Nonphysical sampling distributions in Monte Carlo free-energy estimation: umbrella sampling, J. Comput. Phys. 23 (2) (1977) 187–199, https://doi.org/10.1016/0021-9991(77)90121-8. Feb.
[52] S. Kumar, J.M. Rosenberg, D. Bouzida, R.H. Swendsen, P.A. Kollman, THE weighted histogram analysis method for free-energy calculations on biomolecules. I. THE method, J. Comput. Chem. 13 (8) (1992) 1011–1021, https://doi.org/10.1002/jcc.540130812.
[53] S. Sheridan, F. Gräter, C. Daday, How fast is too fast in force-probe molecular dynamics simulations? J. Phys. Chem. B 123 (17) (2019) 3658–3664, https://doi.org/10.1021/acs.jpcb.9b01251. May 2.
[54] T.A. Wassenaar, K. Pluhackova, R.A. Böckmann, S.J. Marrink, D.P. Tieleman, Going backward: a flexible geometric approach to reverse transformation from coarse grained to atomistic models, J. Chem. Theory Comput. 10 (2) (2014) 676–690, https://doi.org/10.1021/ct400617g. Feb 11.
[55] P. Smith, C.D. Lorenz, LiPyphilic: a Python toolkit for the analysis of lipid membrane simulations, J. Chem. Theory Comput. 17 (9) (2021) 5907–5919, https://doi.org/10.1021/acs.jctc.1c00447. Sep 14.
[56] A.B. Poma, M. Cieplak, P.E. Theodorakis, Combining the MARTINI and structure-based coarse-grained approaches for the molecular dynamics studies of conformational transitions in proteins, J. Chem. Theory Comput. 13 (3) (2017) 1366–1374, https://doi.org/10.1021/acs.jctc.6b00986. Mar 14.
[57] A. Barducci, G. Bussi, M. Parrinello, Well-tempered Metadynamics: a smoothly converging and tunable free-energy method, Phys. Rev. Lett. 100 (2) (2008), https://doi.org/10.1103/PhysRevLett.100.020603, 020603. Jan 18.
[58] W. Kabsch, C. Sander, Dictionary of protein secondary structure: pattern recognition of hydrogen-bonded and geometrical features, Biopolymers 22 (12) (1983) 2577–2637, https://doi.org/10.1002/bip.360221211.
[59] I. Alves, N. Goasdoue, I. Correia, S. Aubry, C. Galanth, S. Sagan, et al., Membrane interaction and perturbation mechanisms induced by two cationic cell penetrating peptides with distinct charge distribution, Biochim. Biophys. Acta Gen. Subj. 1780 (7–8) (2008) 948–959, https://doi.org/10.1016/j.bbagen.2008.04.004. Jul.
[60] A. Mishra, V.D. Gordon, L. Yang, R. Coridan, G.C.L. Wong, HIV TAT forms pores in membranes by inducing saddle-splay curvature: potential role of bidentate hydrogen bonding, Angew. Chem. Int. Ed. 47 (16) (2008) 2986–2989, https://doi.org/10.1002/anie.200704444. Apr 7.
[61] Bouvier B. Curvature as a collective coordinate in enhanced sampling membrane simulations. J. Chem. Theory Comput. 2019Dec 10;15(12):6551–61. doi:https://doi.org/10.1021/acs.jctc.9b00716.
[62] Kauffman WB, Fuselier T, He J, Wimley WC. Mechanism matters: a taxonomy of cell penetrating peptides. Trends Biochem. Sci. 2015Dec;40(12):749–64. doi:https://doi.org/10.1016/j.tibs.2015.10.004.
[63] P. Hänggi, P. Talkner, M. Borkovec, Reaction-rate theory: fifty years after Kramers, Rev. Mod. Phys. 62 (2) (1990) 251–341, https://doi.org/10.1103/RevModPhys.62.251. Apr 1.
[64] T. Harayama, H. Riezman, Understanding the diversity of membrane lipid composition, Nat. Rev. Mol. Cell Biol. 19 (5) (2018) 281–296, https://doi.org/10.1038/nrm.2017.138. May.
[65] S. Sharmin, MdZ Islam, M.A.S. Karal, S.U. Alam Shibly, H. Dohra, M. Yamazaki, Effects of lipid composition on the entry of cell-penetrating peptide Oligoarginine into single vesicles, Biochemistry 55 (30) (2016) 4154–4165, https://doi.org/10.1021/acs.biochem.6b00189. Aug 2.
[66] J. Pae, P. Säälik, L. Liivamägi, D. Lubenets, P. Arukuusk, Ü. Langel, et al., Translocation of cell-penetrating peptides across the plasma membrane is controlled by cholesterol and microenvironment created by membranous proteins, J. Control. Release 192 (2014) 103–113, https://doi.org/10.1016/j.jconrel.2014.07.002. Oct.
[67] A. Lorents, P. Säälik, Ü. Langel, M. Pooga, Arginine-rich cell-penetrating peptides require Nucleolin and cholesterol-poor subdomains for translocation across membranes, Bioconjug. Chem. 29 (4) (2018) 1168–1177, https://doi.org/10.1021/acs.bioconjchem.7b00805. Apr 18.
[68] L. Di, E.H. Kerns, I.F. Bezar, S.L. Petusky, Y. Huang, Comparison of blood–brain barrier permeability assays: *in situ* brain perfusion, MDR1-MDCKII and PAMPA-BBB, J. Pharm. Sci. 98 (6) (2009) 1980–1991, https://doi.org/10.1002/jps.21580. Jun 1.
[69] Javanainen M, Martinez-Seara H, Vattulainen I. Excessive aggregation of membrane proteins in the martini model. PLoS One 2017Nov 13;12(11): e0187936. doi:https://doi.org/10.1371/journal.pone.0187936.
[70] Peng X, Liu X, Kim JY, Nguyen A, Leal J, Ghosh D. Brain-Penetrating Peptide Shuttles across the Blood–Brain Barrier and Extracellular-like Space. Bioconjug. Chem. 2023Dec 20;34(12):2319–36.
[71] N. Kamei, A. Yamaoka, Y. Fukuyama, R. Itokazu, M. Takeda-Morishita, Noncovalent strategy with cell-penetrating peptides to facilitate the brain delivery of insulin through the blood–brain barrier, Biol. Pharm. Bull. 41 (4) (2018) 546–554, https://doi.org/10.1248/bpb.b17-00848.
[72] Crosio MA, Via MA, Cámara CI, Mangiarotti A, Del Pópolo MG, Wilke N. Interaction of a Polyarginine peptide with membranes of different mechanical properties. Biomolecules 2019Oct 18;9(10):625. doi:https://doi.org/10.3390/biom9100625.
[73] A.D. Robison, S. Sun, M.F. Poyton, G.A. Johnson, J.P. Pellois, P. Jungwirth, et al., Polyarginine interacts more strongly and cooperatively than Polylysine with phospholipid bilayers, J. Phys. Chem. B 120 (35) (2016) 9287–9296, https://doi.org/10.1021/acs.jpcb.6b05604. Sep 8.
[74] J.M. Swiecicki, A. Bartsch, J. Tailhades, M. Di Pisa, B. Heller, G. Chassaing, et al., The efficacies of cell-penetrating peptides in accumulating in large Unilamellar vesicles depend on their ability to form inverted micelles, ChemBioChem 15 (6) (2014) 884–891, https://doi.org/10.1002/cbic.201300742.
[75] MdZ Islam, S. Sharmin, Md Moniruzzaman, M. Yamazaki, Elementary processes for the entry of cell-penetrating peptides into lipid bilayer vesicles and bacterial cells, Appl. Microbiol. Biotechnol. 102 (9) (2018) 3879–3892, https://doi.org/10.1007/s00253-018-8889-5. May 1.
[76] N. Sakai, S. Matile, Anion-mediated transfer of Polyarginine across liquid and bilayer membranes, J. Am. Chem. Soc. 125 (47) (2003) 14348–14356, https://doi.org/10.1021/ja037601l. Nov.
[77] MdMR Moghal, MdZ Islam, F. Hossain, S.K. Saha, M. Yamazaki, Role of membrane potential on entry of cell-penetrating peptide Transportan 10 into single vesicles, Biophys. J. 118 (1) (2020) 57–69, https://doi.org/10.1016/j.bpj.2019.11.012. Jan 7.
[78] M. Hasan, MdMR Moghal, S.K. Saha, M. Yamazaki, The role of membrane tension in the action of antimicrobial peptides and cell-penetrating peptides in biomembranes, Biophys. Rev. 11 (3) (2019) 431–448, https://doi.org/10.1007/s12551-019-00542-1. May 15.
[79] J.D. Richardson, R.C. Van Lehn, Free energy analysis of peptide-induced pore formation in lipid membranes by bridging atomistic and coarse-grained simulations, J. Phys. Chem. B 128 (36) (2024) 8737–8752, https://doi.org/10.1021/acs.jpcb.4c03276. Sep 12.
[80] C. Allolio, A. Magarkar, P. Jurkiewicz, K. Baxová, M. Javanainen, P.E. Mason, et al., Arginine-rich cell-penetrating peptides induce membrane multilamellarity and subsequently enter via formation of a fusion pore, Proc. Natl. Acad. Sci. 115 (47) (2018) 11923–11928, https://doi.org/10.1073/pnas.1811520115. Nov 20.
[81] Z. Chen, R.P. Rand, The influence of cholesterol on phospholipid membrane curvature and bending elasticity, Biophys. J. 73 (1) (1997) 267–276, https://doi.org/10.1016/S0006-3495(97)78067-6. Jul.
[82] A. Krishna, D. Sengupta, Interplay between membrane curvature and cholesterol: role of Palmitoylated Caveolin-1, Biophys. J. 116 (1) (2019) 69–78, https://doi.org/10.1016/j.bpj.2018.11.3127. Jan 8.
[83] N. Schmidt, A. Mishra, G.H. Lai, G.C.L. Wong, Arginine-rich cell-penetrating peptides, FEBS Lett. 584 (9) (2010) 1806–1813, https://doi.org/10.1016/j.febslet.2009.11.046.
[84] P.K. Lai, Y.N. Kaznessis, Insights into membrane translocation of Protegrin antimicrobial peptides by multistep molecular dynamics simulations, ACS Omega 3 (6) (2018) 6056–6065, https://doi.org/10.1021/acsomega.8b00483. Jun 30.
[85] S. Choe, Translocation of a single Arg $$_9$$ peptide across a DOPC/DOPG(4:1) model membrane using the weighted ensemble method, Sci. Rep. 13 (1) (2023) 1168, https://doi.org/10.1038/s41598-023-28493-4. Jan 20.
[86] E. Fattal, S. Nir, R.A. Parente, F.C. Szoka, Pore-forming peptides induce rapid phospholipid Flip-flop in membranes, Biochemistry 33 (21) (1994) 6721–6731, https://doi.org/10.1021/bi00187a044. May 1.
[87] A.E. Cardenas, R. Elber, Membrane-embedded anti-Cancer peptide causes a minimal structural perturbation that is sufficient to enhance phospholipid Flip-flop and charge permeation rates, Life 15 (7) (2025), https://doi.org/10.3390/life15071007. Jun 25.

[88] K.R. Applegate, J.A. Glomset, Computer-based modeling of the conformation and packing properties of docosahexaenoic acid, J. Lipid Res. 27 (6) (1988) 658–680, https://doi.org/10.1016/S0022-2275(20)38805-2. Aug.
[89] R. Baccouch, Y. Shi, E. Vernay, M. Mathelié-Guinlet, N. Taib-Maamar, S. Villette, et al., The impact of lipid polyunsaturation on the physical and mechanical properties of lipid membranes. Biochimica et Biophysica Acta (BBA), Biomembranes 1865 (2) (2023), https://doi.org/10.1016/j.bbamem.2022.184084, 184084. Feb.
[90] A. Roux, D. Cuvelier, P. Nassoy, J. Prost, P. Bassereau, B. Goud, Role of curvature and phase transition in lipid sorting and fission of membrane tubules, EMBO J. 24 (8) (2005) 1537–1545, https://doi.org/10.1038/sj.emboj.7600631. Apr 20.
[91] S. Mukherjee, T.T. Soe, F.R. Maxfield, Endocytic sorting of lipid analogues differing solely in the chemistry of their hydrophobic tails, J. Cell Biol. 144 (6) (1999) 1271–1284, https://doi.org/10.1083/jcb.144.6.1271. Mar 22. (PubMed PMID: 10087269).
[92] W. Rawicz, K.C. Olbrich, T. McIntosh, D. Needham, E. Evans, Effect of chain length and unsaturation on elasticity of lipid bilayers, Biophys. J. 79 (1) (2000) 328–339, https://doi.org/10.1016/S0006-3495(00)76295-3. Jul.
[93] M.C. Morris, P. Vidal, L. Chaloin, F. Heitz, G. Divita, A new peptide vector for efficient delivery of oligonucleotides into mammalian cells, Nucleic Acids Res. 25 (14) (1997) 2730–2736, https://doi.org/10.1093/nar/25.14.2730. Jul 1.
[94] Bozelli JC, Epand RM. Membrane shape and the regulation of biological processes. J. Mol. Biol. 2020Aug 21;Molecular Mechanisms in Integral Membrane Enzymology432(18):5124–36. doi:https://doi.org/10.1016/j.jmb.2020.03.028.
[95] K.L. Baxová, J. Koikkara, C. Allolio, From molecular insight to mesoscale membrane remodeling: curvature generation by arginine-rich cell-penetrating peptides, bioRxiv (2025), https://doi.org/10.1101/2025.04.14.648709. Jan 1; 2025.04.14.648709.
[96] H.D. Herce, A.E. Garcia, Molecular dynamics simulations suggest a mechanism for translocation of the HIV-1 TAT peptide across lipid membranes, Proc. Natl. Acad. Sci. 104 (52) (2007) 20805–20810, https://doi.org/10.1073/pnas.0706574105. Dec 26.
[97] K.L. Baxová, J. Koikkara, C. Allolio, From molecular insight to mesoscale membrane remodeling: curvature generation by arginine-rich cell-penetrating peptides, bioRxiv (2025), https://doi.org/10.1101/2025.04.14.648709. Jan 1; 2025.04.14.648709.
[98] M. Doktorova, H. Weinstein, Accurate in silico modeling of asymmetric bilayers based on biophysical principles, Biophys. J. 115 (9) (2018) 1638–1643, https://doi.org/10.1016/j.bpj.2018.09.008. Nov 6.
[99] G. Khelashvili, B. Kollmitzer, P. Heftberger, G. Pabst, D. Harries, Calculating the bending Modulus for multicomponent lipid membranes in different thermodynamic phases, J. Chem. Theory Comput. 9 (9) (2013) 3866–3871, https://doi.org/10.1021/ct400492e. Sep 10.
[100] S. Deshayes, T. Plénat, G. Aldrian-Herrada, G. Divita, C. Le Grimellec, F. Heitz, Primary amphipathic cell-penetrating peptides: structural requirements and interactions with model membranes, Biochemistry 43 (24) (2004) 7698–7706, https://doi.org/10.1021/bi049298m. Jun 1.
[101] Mitchell D j., Steinman L, Kim D t., Fathman C g., Rothbard J b. Polyarginine enters cells more efficiently than other polycationic homopolymers. J. Pept. Res. 2000;56(5):318–25. doi:https://doi.org/10.1034/j.1399-3011.2000.00723.x.
[102] P.A. Wender, D.J. Mitchell, K. Pattabiraman, E.T. Pelkey, L. Steinman, J. B. Rothbard, The design, synthesis, and evaluation of molecules that enable or enhance cellular uptake: Peptoid molecular transporters, Proc. Natl. Acad. Sci. 97 (24) (2000) 13003–13008, https://doi.org/10.1073/pnas.97.24.13003. Nov 21.
[103] M. Vazdar, J. Heyda, P.E. Mason, G. Tesei, C. Allolio, M. Lund, et al., Arginine "magic": Guanidinium like-charge ion pairing from aqueous salts to cell penetrating peptides, Acc. Chem. Res. 51 (6) (2018) 1455–1464, https://doi.org/10.1021/acs.accounts.8b00098. Jun 19.
[104] E. Eiríksdóttir, K. Konate, Ü. Langel, G. Divita, S. Deshayes, Secondary structure of cell-penetrating peptides controls membrane interaction and insertion. Biochimica et Biophysica Acta (BBA), Biomembranes 1798 (6) (2010) 1119–1128, https://doi.org/10.1016/j.bbamem.2010.03.005. Jun 1.
[105] C.M. Dunkin, A. Pokorny, P.F. Almeida, H.S. Lee, Molecular dynamics studies of Transportan 10 (Tp10) interacting with a POPC lipid bilayer, J. Phys. Chem. B 115 (5) (2011) 1188–1198, https://doi.org/10.1021/jp107763b. Feb 10.
[106] Lai AL, Moorthy AE, Li Y, Tamm LK. Fusion activity of HIV gp41 fusion domain is related to its secondary structure and depth of membrane insertion in a cholesterol-dependent fashion. J. Mol. Biol. 2012Apr 20;418(0):https://doi.org/10.1016/j.jmb.2012.02.010. doi:https://doi.org/10.1016/j.jmb.2012.02.010.
[107] F. Madani, S. Lindberg, Ü. Langel, S. Futaki, A. Gräslund, Mechanisms of cellular uptake of cell-penetrating peptides, J Biophys. 2011 (2011) 414729, https://doi.org/10.1155/2011/414729.
[108] I. Ruseska, A. Zimmer, Internalization mechanisms of cell-penetrating peptides, Beilstein J. Nanotechnol. 9 (11) (2020) 101–123, https://doi.org/10.3762/bjnano.11.10. Jan.
[109] M.J. Abraham, T. Murtola, R. Schulz, S. Páll, J.C. Smith, B. Hess, E. Lindahl, GROMACS: High performance molecular simulations through multi-level parallelism from laptops to supercomputers, SoftwareX 1–2 (2015) 19–25, https://doi.org/10.1016/j.softx.2015.06.001.